Fragment Correlation in the Three-Body Breakup of Triatomic Hydrogen

U. Müller, Th. Eckert, M. Braun, and H. Helm

Universität Freiburg, Fakultät für Physik, Hermann-Herder-Strasse 3, D-79104 Freiburg, Germany
(Received 3 March 1999)

We investigate the fragmentation of the triatomic hydrogen molecule H_3 in a triple-coincidence experiment. A single rovibronic state of H_3 is laser prepared and its breakup into three hydrogen atoms $H(1s)$ is monitored by time- and position-sensitive multihit detectors. For each triple hit, the momentum vectors of the three $H(1s)$ fragments are determined. The sixfold differential cross section of the fragment momentum components in the center-of-mass frame is found to be highly structured and to depend sensitively on the H_3 initial electronic state.

The triatomic hydrogen molecule as the prototype for a polyatomic molecule has attracted the interest of physicists and chemists for many decades. Numerous reactive scattering experiments were performed to explore the repulsive ground state potential energy surface of H_3 and their results were found to agree with *ab initio* theoretical predictions [1,2]. Bound Rydberg states of the H_3 molecule exist. They were first discovered by Herzberg's group [3] and have since been studied extensively [4]. These states can undergo radiative as well as predissociative decay processes into the ground state dissociation continuum. Continuous photoemission spectra from $n = 3$ Rydberg states of H_3 have been observed [5,6] giving insight into the fs-decay dynamics on both sheets of the ground state surface [7] and highlighting the importance of the upper sheet which correlates asymptotically to $H(1s) + H(1s) + H(1s)$. The predissociation of laser-prepared H_3 into $H + H_2(v, J)$ fragment pairs was investigated by translational spectroscopy [8,9]. The initial- and final-state resolved experimental data were compared to wave-packet calculations [10] giving insight into the coupling mechanisms between the excited and ground state surfaces in the regime of the breakdown of the Born-Oppenheimer approximation.

A most intriguing feature of H_3 is the breakup into three ground state hydrogen atoms. This is an open decay channel for all electronically excited states of H_3. For larger molecules, three-body decay may constitute a major fragmentation pathway and has come into the focus of recent investigations [11–14]. In the case of H_3, Peterson *et al.* [15] found evidence for this process in dissociative charge transfer of H_3^+ in Cs, and Datz *et al.* [16] measured the branching between two-body and three-body channels in dissociative recombination of H_3^+ with electrons. Three-body decay of laser-prepared Rydberg states of H_3 was discovered by translational spectroscopy where two fragments were detected in coincidence [17]. The fragmentation of a molecule into three neutral atoms slowly receding from the center of mass opens the possibility to experimentally study the correlation of the fragment momentum vectors. The fragment trajectories are not affected by long-range postcollisional interaction as in the case of

breakup into three charged particles [18]. The correlation of the neutral fragment momenta reflects the decay dynamics when entering into and evolving on the repulsive potential energy surfaces. Such an experiment is reported here.

The investigations are performed with a novel photofragmentation spectrometer which is an advanced version of earlier forms [19,20]. A fast neutral beam of H_3 molecules in the single long-lived rotational state $2p\ ^2A_2''(N = K = 0)$ is produced by charge transfer of 3 keV H_3^+ ions in cesium. Unreacted ions are removed by an electric field and the products of dissociative charge transfer are stopped by a 100 μm diameter aperture located 30 cm downstream of the charge transfer cell. The well-collimated neutral beam (measured divergence 1.5 mrad FWHM) is then crossed by an intracavity dye laser beam. The laser is tuned to excite transitions from the metastable $2p\ ^2A_2''(N = K = 0)$ into the vibrationless $3s\ ^2A_1'(N = 1, K = 0)$ or $3d\ ^2E''(N = 1, G = 0, R = 1)$ Rydberg states of H_3 at frequencies of 16 695 and 17 297 cm^{-1}, respectively. The excited states are known to decay in radiative and predissociative channels within 3 to 10 ns [8]. The undissociated part of the neutral beam is intercepted by a beam flag at a distance of 10 cm from the laser-interaction region. After the free flight of 1.5 m, photofragments are detected in coincidence by a time- and position-sensitive multihit detector (Fig. 1). The detector consists of two identical units mounted above and below the neutral beam path. The units consist of pairs of multichannel plates followed by delay line-type position-sensitive anodes developed in the Frankfurt group [21]. Each anode is formed by two waveguides, one for each Cartesian coordinate. Electromagnetic pulses excited by the charge cloud from the microchannel plates travel to the waveguide terminals where they are converted to NIM-standard pulses by differential amplifiers and constant-fraction discriminators. The hit position on the detector surface is coded into the pulse arrival times at the waveguide ends monitored by time-to-digital converters (TDC) with 25 ps resolution. The TDC's are triggered by timing pulses derived from the current surge in the multichannel plates. Pulse routers distribute the signals from each waveguide

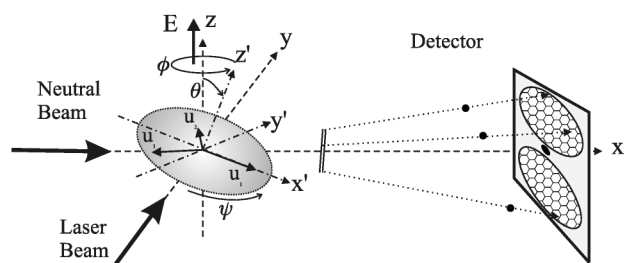0031-9007/99/83(14)/2718(4)$15.00

FIG. 1. Geometry of the photofragmentation experiment for the detection of three-body breakup of the triatomic hydrogen molecule. The coordinate frames relevant for the reduction of the sixfold differential cross section of the fragment momentum vectors are shown.

end into two separate TDC channels, respectively. A similar design allows for the detection of double events on the timing signals. Each unit is capable of detecting consecutive fragments with a dead time as low as 10 ns. Additional TDC channels allow us to determine the arrival time differences between events on the two detector sides. The readout and preanalysis of the data are performed by a dedicated processor. A double hit on one detector half and a single hit on the other half appearing within a 400 ns wide time window are recognized as a possible three-body event. From the 14 binary TDC values, the six Cartesian coordinates of the three impact positions in the detector plane and the two arrival time differences of the three impact times are determined. Redundant information on the arrival time differences is used to reject false coincidences. False events produced by ion feedback in the microchannel plates are discriminated against by their spatial proximity.

In the next step, we calculate for each three-body event the three fragment momenta $m\mathbf{u}_1$, $m\mathbf{u}_2$, and $m\mathbf{u}_3$ in the center-of-mass frame (see Fig. 1) making use of the well-known primary beam energy, the parent mass, and the flight distance between the interaction region and the detector. Momentum conservation requires that $\mathbf{u}_1 + \mathbf{u}_2 + \mathbf{u}_3 = 0$ which implies that the three momentum vectors have only six independent components. This allows us to additionally determine for each dissociation event the velocity components of the center-of-mass motion perpendicular to the neutral beam. This latter information is also used to reject false coincidences. In this way, we determine the sixfold differential cross section, completely characterizing the final state of the three-body decay process.

In the following, we consider suitable projections of this high-dimensional set of information to gain insight into the fragmentation pattern. First, we accumulate spectra of the total c.m. kinetic energy release $W = m(\mathbf{u}_1^2 + \mathbf{u}_2^2 + \mathbf{u}_3^2)/2$. Figure 2 shows kinetic energy release spectra from triple-coincidence data of the H_3 $3s$ $^2A_1'(N = 1, K = 0)$ and $3d$ $^2E''(N = 1, G = 0, R = 1)$ initial states binned at 10 meV resolution. In the spectrum of the $3s$ state (Fig. 2a), a narrow peak appears at 3.17 eV which is close to the known energy of the initial state above the three-body limit, 3.155 eV [8]. The kinetic energy

spectrum of the $3d$ $^2E''$ state (Fig. 2b) shows a strong peak at 3.23 eV which corresponds to the breakup of the initial state into three hydrogen atoms, expected at a position of 3.230 eV. The peak at 2.71 eV results from three-body breakup following the radiative transition $3d$ $^2E'' \rightarrow 3p$ $^2E'$ [3]. The excellent agreement between measured absolute values of W and the previously known state energies confirms the quality of the absolute energy calibration of the detector which was carried out with calibrated position masks [22]. No continuous background is found in the kinetic energy release spectra in Fig. 2. This shows that radiative transitions from the $3s$ $^2A_1'$ and $3d$ $^2E''$ states to the repulsive ground state lead to $H + H_2$ fragment pairs as the only exit channel [9]. It also indicates that the continuous photoemission spectra observed by Bruckmeier et al. [5] and by Raksit et al. [6] are accompanied by two-body decay.

In order to project the high-dimensional data sets, we introduce six parameters which uniquely describe the three fragment momentum vectors (cf. Fig. 1). The $\mathbf{u}_i$ are contained in a plane. For each event, we define a new coordinate system (x', y', z') by the normal vector on this plane (z' axis) and the direction of the largest momentum vector observed (x' axis). Three Euler angles (ψ, θ, ϕ) describe the orientation of the (x', y', z')-coordinate system within the laboratory reference system (x, y, z), defined by the electric vector of the laser beam (z axis) and the direction of the neutral beam (x axis). For the remaining three parameters describing the arrangement of the three momenta in the (x', y') plane we may choose the absolute values of the momenta $p_i = m|\mathbf{u}_i|$ or the individual fragment energies $\epsilon_i = m\mathbf{u}_i^2/2$. We use the total kinetic energy W and two parameters showing the correlation among the fragment momenta. These could be two angles between the momentum vectors. We could
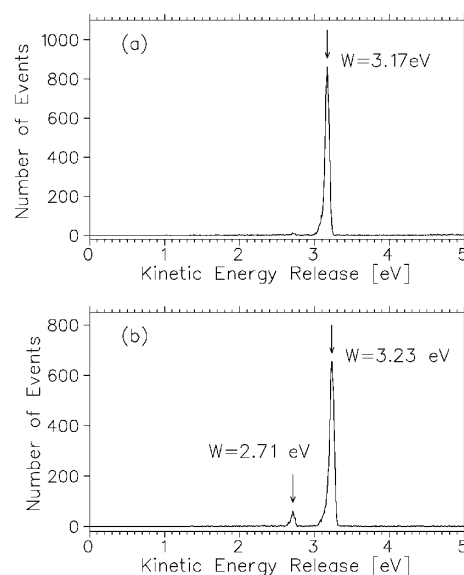

FIG. 2. Kinetic energy release in the three-body decay of the $3s$ $^2A_1'$ (a) and $3d$ $^2E''$ (b) states of H_3.
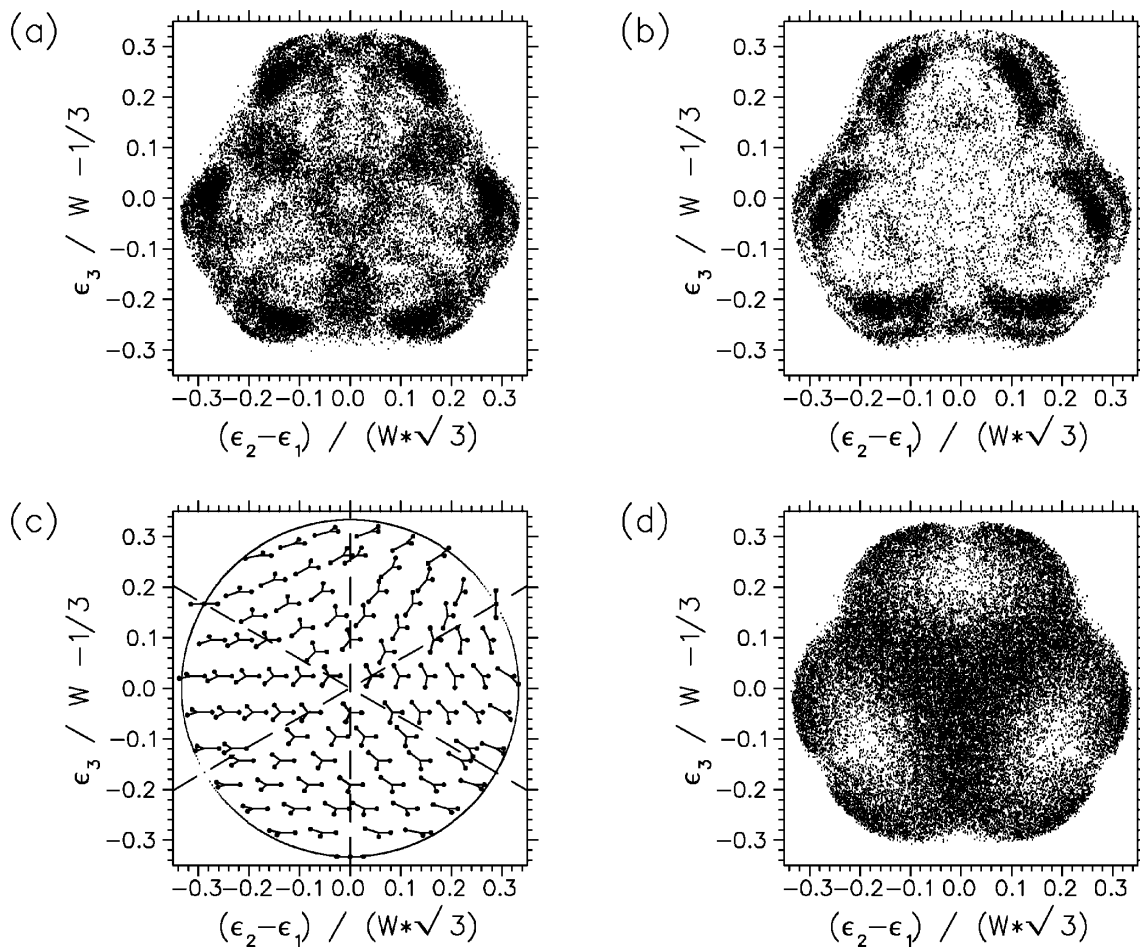
FIG. 3. Dalitz plot of the raw data from three-body decay of the $3s\ ^2A_1'$ (a) and $3d\ ^2E''$ (b) initial states of H_3. In (c), the correspondence between the location in the plot and the fragmentation configuration is indicated. In (d) a Monte Carlo simulation for a random distribution of fragmentation configuration in the phase space is shown, demonstrating the effect of the geometric detector collection efficiency.

also plot the (x', y') momentum vector components of the fragment with the smallest energy normalized to the absolute momentum of the fastest fragment. We prefer to use a Dalitz plot [23] because in this representation the phase space density is conserved meaning that a fragmentation process with a matrix element independent of the configuration leads to a homogeneous distribution in the space of the kinematically allowed region. Preferred fragmention pathways can be immediately recognized from the point density in such a plot. To obtain a Dalitz plot we plot for each event $(\epsilon_3/W - 1/3)$ vs $[(\epsilon_2 - \epsilon_1)/(W\sqrt{3})]$. Energy and momentum conservation require that the data points in this plot lie inside a circle with radius $1/3$, centered at the origin.

In Figs. 3a and 3b, the triple-coincident events following three-body breakup of the laser-excited H_3 $3s\ ^2A_1'(N = 1, K = 0)$ and $3d\ ^2E''(N = 1, G = 0, R = 1)$ states are shown as Dalitz plots, selecting only events within the narrow kinetic energy regions around the peaks in Fig. 2 (3.05 to 3.25 eV and 3.1 to 3.35 eV, respectively). Since the three hydrogen atoms are indistinguishable, points are drawn in Fig. 3 for the six permutations of the fragment energies ϵ_i measured in each event. In Fig. 3c, the correspondence between the configuration of the fragment momenta and the location in the plot is visualized. The threefold rotation symmetry around the origin and the mirror symmetry with respect to the dashed lines in Fig. 3c result from the equal masses of the fragments. In order to understand the meaning of the very pronounced islands of correlation appearing in the experimental data in Figs. 3a and 3b, the limited collection efficiency of the detector has to be discussed first. Currently, detection of fragment triples where one of the momenta is close to zero (linear configuration) and therefore hits the space between the two detectors is excluded. Also, fragment hits which are close in time as well as in space ($H + H_2$ configuration) are suppressed due to the finite pulse pair resolution of 10 ns. The geometric and electronic detector collection efficiency was determined in a Monte Carlo simulation by generating a uniform distribution of fragmentation configurations and calculating the fragment propagation to the detector. The simulation requires as a vital input information on the distribution of the angles θ, ψ, and ϕ.

By appropriately projecting the experimental data sets and comparing them with the results of the Monte Carlo simulation, we determine the alignment parameter β describing the probability distribution of the angle θ by $P(\cos\theta) = [1 + \beta(3\cos^2\theta - 1)/2]/(4\pi)$ [24]. We find $\beta = 2^{+0}_{-0.2}$ for the $3s\ ^2A'_1$ state and $\beta = 0^{+0.2}_{-0}$ for the $3d\ ^2E''$ state. The alignment of the z' axis corresponds to that of the molecular top axis described by $\beta = 2$ and $\beta = 0.2$ for the laser-prepared $3s\ ^2A'_1$ and $3d\ ^2E''$ initial states, respectively [17]. This shows that the plane of the fragment momenta is determined by the orientation of the molecular plane. The experimentally observed uniform distributions of the angles ψ and ϕ are expected from the rotational symmetries about the molecular top axis and the electric vector of the laser field. A Monte Carlo simulation of the detector response for $\beta = 0.2$ is shown in Fig. 3d. The collection efficiency vanishes only for the linear and the H + H$_2$ configurations on the circle boundary. The remainder of the Dalitz plot area shows a smooth variation of the detection efficiency.

As a consequence, the islands of high point density in Figs. 3a and 3b are associated with the correlation of the fragment momenta produced by the dissociation process itself. Despite the high symmetry (D_{3h}) of the initial states, asymmetric fragmentation configurations are very much preferred in finding a path into the 3-particle continuum. Neither the totally symmetric configuration (center of the plot) nor isosceles configurations (dashed lines in Fig. 3c) show emphasized population. It may be surprising, that the preferred fragmentation configurations sensitively depend on the initial state, although the absolute energies of the states investigated here differ as little as 75 meV, and the nuclear equilibrium configuration for each initial state is extremely close to that of the vibrationless H$_3^+$ ion in its ground electronic state. The striking difference of the final-state distributions must reflect the different coupling mechanisms between the initial state and the two sheets of the repulsive ground state potential energy surface. The breakdown of the Born-Oppenheimer approximation is mediated by the zero-point motion in the degenerate vibration for the $3s\ ^2A'_1$ state, and by the rotational tumbling motion in case of the $3d\ ^2E''$ state [17]. While these processes mediate the first entry of the quasibound system into the continuum, a series of avoided crossings between the upper sheet of the repulsive ground state surface and the s- and d-Rydberg states of $2\Sigma_g^+$ symmetry in linear geometry (Petsalakis *et al.* [25]) governs the further evolution of the continuum state. As a consequence, the detailed maps of momentum partition among the three fragments obtained in our experiment pose a significant challenge to quantum-structure and quantum-dynamics calculations.

[1] A. Kuppermann and Y.-S. M. Wu, Chem. Phys. Lett. **241**, 229 (1995).

[2] L. Bañares, F. J. Aoiz, V. J. Herrero, M. J. D'Mello, B. Niederjohann, K. Seekamp-Rahn, E. Wrede, and L. Schnieder, J. Chem. Phys. **108**, 6160 (1998).

[3] G. Herzberg, J. T. Hougen, and J. K. G. Watson, Can. J. Phys. **60**, 1261 (1982).

[4] U. Müller, U. Majer, R. Reichle, and M. Braun, J. Chem. Phys. **106**, 7958 (1997), and references therein.

[5] R. Bruckmeier, Ch. Wunderlich, and H. Figger, Phys. Rev. Lett. **72**, 2550 (1994); D. Azinovic, R. Bruckmeier, Ch. Wunderlich, and H. Figger, Phys. Rev. A **58**, 1115 (1998).

[6] A. B. Raksit, R. F. Porter, W. P. Garver, and J. J. Leventhal, Phys. Rev. Lett. **55**, 378 (1985).

[7] S. Mahapatra and H. Köppel, J. Chem. Phys. **109**, 1721 (1998).

[8] P. C. Cosby and H. Helm, Phys. Rev. Lett. **61**, 298 (1988).

[9] U. Müller and P. C. Cosby, J. Chem. Phys. **105**, 3532 (1996).

[10] J. L. Krause, K. C. Kulander, J. C. Light, and A. E. Orel, J. Chem. Phys. **96**, 4283 (1992); J. L. Krause, A. E. Orel, B. H. Lengsfield, and K. C. Kulander, in *Time-Dependent Quantum Molecular Dynamics,* edited by J. Broeckhove and L. Lathouwers (Plenum, New York, 1992), p. 131.

[11] C. Maul, T. Haas, and K. H. Gericke, J. Phys. Chem. A **101**, 6619 (1997).

[12] Y. Tanaka, M. Kawaski, Y. Matsumi, H. Fujiwara, T. Ishiwata, L. J. Rogers, R. N. Doxin, and M. N. R. Ashfold, J. Chem. Phys. **109**, 1315 (1998).

[13] J. J. Lin, D. W. Hwang, Y. T. Lee, and X. Yang, J. Chem. Phys. **108**, 10 061 (1998).

[14] M. Lange, O. Pfaff, U. Müller, and R. Brenn, Chem. Phys. **230**, 117 (1998).

[15] J. R. Peterson, P. Devynck, Ch. Hertzler, and W. G. Graham, J. Chem. Phys. **96**, 8128 (1992).

[16] S. Datz, G. Sundström, Ch. Biedermann, L. Broström, H. Danared, S. Mannervik, J. R. Mowat, and M. Larsson, Phys. Rev. Lett. **74**, 896 (1995).

[17] U. Müller and P. C. Cosby, Phys. Rev. A **59**, 3632 (1999).

[18] L. M. Wiese, O. Yenen, B. Thaden, and D. H. Jaecks, Phys. Rev. Lett. **79**, 4982 (1997).

[19] D. P. de Bruin and J. Los, Rev. Sci. Instrum. **53**, 1020 (1982).

[20] H. Helm and P. C. Cosby, J. Chem. Phys. **86**, 6813 (1987).

[21] O. Jagutzki, V. Mergel, K. Ullmann-Pfleger, L. Spielberger, U. Meyer, and H. Schmidt-Böcking, in Imaging Spectroscopy IV, SPIE Proceedings (SPIE– International Society for Optical Engineering, Bellingham, WA, to be published).

[22] M. Braun, Ph.D. thesis, Freiburg, 1999.

[23] R. H. Dalitz, Philos. Mag. **44**, 1068 (1953); Annu. Rev. Nucl. Sci. **13**, 339 (1963).

[24] R. N. Zare, Ber. Bunsen-Ges. Phys. Chem. **86**, 422 (1982).

[25] I. D. Petsalakis, G. Theodorakopoulos, and J. S. Wright, J. Chem. Phys. **89**, 6850 (1988).